# Science

**AAAS**

# Abrupt Temperature Changes in the Western Mediterranean over the Past 250,000 Years

Belen Martrat,[1] Joan O. Grimalt,[1]* Constancia Lopez-Martinez,[1]
Isabel Cacho,[1,2] Francisco J. Sierro,[3] Jose Abel Flores,[3]
Rainer Zahn,[2] Miquel Canals,[2] Jason H. Curtis,[4] David A. Hodell[4]

A continuous high-resolution Western Mediterranean sea surface temperature (SST) alkenone record spanning the past 250,000 years shows that abrupt changes were more common at warming than at cooling. During marine isotope stage (MIS) 6, SST oscillated following a stadial-interstadial pattern but at lower intensities and rates of change than in the Dansgaard/Oeschger events of MIS 3. Some of the most prominent events occurred over MISs 5 and 7, after prolonged warm periods of high stability. Climate during the whole period was predominantly maintained in interglacial-interstadial conditions, whereas the duration of stadials was much shorter.

Northern Hemisphere submillennial-scale climate variations during the last glacial have been documented in Greenland ice (1–3), marine and continental sediments (4–14), and stalagmites (15, 16). Some of these records also suggest that high-frequency climate variability was not restricted to this period (6–7, 10–14, 16). However, because of the lack of high-resolution marine data, very little is known about the climate history of the penultimate glacial. The deepest sections of the Greenland ice cores that cover this time interval are distorted by basal deformation (2, 3). The sediments from site 977A, leg 161 of the Ocean Drilling Program (ODP), examined in this study at a time resolution of 386 ± 131 years for the past 250 thousand years (ky) may help provide better understanding of millennial scale variability over those periods.

Core ODP-977A was retrieved from the eastern subbasin of the Alboran Sea (Fig. 1). The $\delta^{18}O$ record of *Globigerina bulloides* displays a well-defined orbital modulation of glacial and interglacial marine isotope stages (MISs) (17, 18) (Fig. 2, A and B). Between 80 and 11.5 thousand years ago (ka) it also shows remarkable consistency with the Dansgaard/Oeschger (D/O) cycles observed in Greenland $\delta^{18}O$ profiles (1–3) (Fig. 2H). Over the past 250 ky before the present, sea surface temperature (SST) derived from the

$U^{k'}_{37}$ alkenone index (Fig. 2D) displays characteristic sequences of rapid warming and cooling events, here labeled as Alboran interstadials (AI-1 to AI-26 and AI-1' to AI-15' for the last and penultimate climate cycles, respectively) and stadials (AS-1 to AS-26 and AS-1' to AS-15', respectively) (19, 20). Most SST changes occurred simultaneously with the variations in the $\delta^{18}O$ record of *G. bulloides*. Thus, temporal offsets due to dissimilar sedimentation processes between coccolithophores and foraminifera (21) appear not to be important at this site. The section between 50 and 0 ka displays SST variability similar to that in core MD95-2043, analyzed in a previous study (8). Parallel changes, both in terms of frequency

and amplitude, have been observed during the last climate cycle from lower to higher latitudes in the Northern Hemisphere (5, 9, 10, 22, 23), suggesting that ODP site 977A may provide representative SST patterns on a broad regional scale.

During MIS 3, SST varied by up to 6°C within less than 1 ky after the abrupt D/O events in Greeland Ice Core Project (GRIP) (Fig. 2, D and H). Technically, abrupt climate changes occur when the climate system is forced to cross a threshold, triggering a transition into a new climate condition at a rate faster than the cause (24). The magnitude of the change caused by system feedbacks often appears as large as or larger than that due to the major direct climate forcings (25). From a more operational standpoint, paleoclimatic changes in marine systems can be compared to SST variation over the last deglaciation, i.e., an average warming of 2.6°C/ky in core ODP-977A [7.5°C in 2.9 ky (table S1)]. Thus, in the present study, abrupt SST change refers to warming or cooling episodes that happened at a rate equal to or faster than the average. Evaluation of SST during MISs 2 to 4 under this criterion shows twice as many abrupt warmings as cooling episodes (Fig. 2D). Uncertainties associated with core sampling or age modeling could lead to some variation in the absolute number of these abrupt SST changes, but the higher number of abrupt warming events is a robust feature. $\delta^{18}O$ in Greenland ice cores also shows a characteristic pattern of abrupt warming followed by gradual cooling (1–3).

Six SST minima in core ODP-977A [AS-2a, 2c, 5, 9, 13, and 18 (Fig. 2D)] are concurrent with the periods of massive iceberg
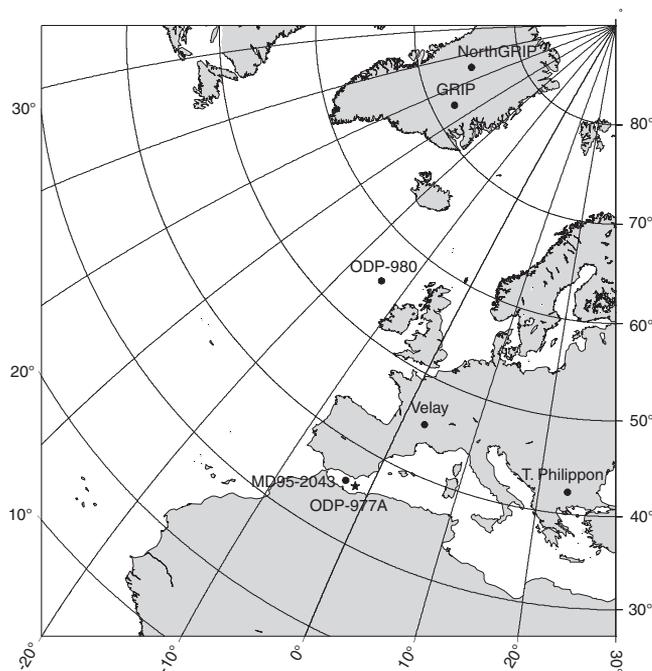


**Fig. 1.** Map showing the location of core ODP site 977A in the Alboran Sea. The locations of other paleoclimate sites mentioned in the text are also shown. MD95-2043 (8) and GRIP (1) were used for the age model for the past 80 ky (17). The Velay and the Tenaghi Philippon long pollen sequences (13, 14) document the terrestrial response to climate at a time resolution of millennia. Also, the location of core ODP site 980 is indicated as an excellent archive of catastrophic iceberg discharges (6).

[1]Department of Environmental Chemistry Institut d'Investigacions Quimiques i Ambientals de Barcelona–Consell Superior d'Investigacions Cientifiques (CSIC), 08034-Barcelona, Spain. [2]Department of Stratigraphy, Paleontology, and Marine Geosciences, University of Barcelona, 08028-Barcelona, Spain. [3]Department of Geology, University of Salamanca, 37008-Salamanca, Spain. [4]Department of Geological Sciences, University of Florida, Gainesville, FL 32611–2120, USA.

*To whom correspondence should be addressed. E-mail: jgoqam@cid.csic.es

production and melting called Heinrich events (HEs), which lead to the deposition in the Atlantic Ocean of sediment layers dominated by detritic particles larger than 150 μm (4, 26). The abrupt changes associated with HEs were also more common in increases than in decreases of SST, for example, three warmings (AS-2a ≈ H1, AS-9 ≈ H4, and AS-13 ≈ H5) and one cooling [AS-2c ≈ H2 (Fig. 2D and table S1)]. The Heinrich layers are found in the open North Atlantic (4, 6) (Fig. 2G), the Nordic seas (5), and the western Iberian margin (11, 27), but there is no evidence of transportation of ice-rafted detritus (IRD) into the Mediterranean Sea. In the Alboran Sea, the SST drops

associated with HE show coeval increases in the relative proportion of the polar planktonic foraminifera *Neogloboquadrina pachyderma* (sinistral) to total foraminifera (8, 28) and in the relative proportion of the tetraunsaturated $C_{37}$ alkenone homolog, $C_{37:4}$, to total $C_{37}$ alkenones (Fig. 2C). Increased abundance in $C_{37:4}$ is consistent with a previous study from the western Iberian margin showing that this compound indicates an influence of low-salinity water masses during such events (29). In this respect, the two SST drops between 25 and 20 ka in core ODP-977A, AS-2c, and AS-3 [which coincide with GS-2c and GS-3 in GRIP, respectively (Fig. 2, D and H)] can be differentiated by the $C_{37:4}$ content. Both

cooling events were also observed off the west Iberian coast, and only the AS-2c was correlated with increased IRD (29). Thus, the AS-3 event, the lowest SST value of the whole ODP-977A record, is not related to a HE but corresponds to a well-defined δ18O minimum in GRIP. The similarity between SST values in ODP-977A and GRIP points to a teleconnection between high and midlatitudes in the Northern Hemisphere that is unrelated to iceberg discharges.

Although less frequent than during MIS 2 to 4, millennial-scale variability over MIS 6 is also observed in core ODP-977A. In MIS 6 only three SST changes can be considered as abrupt, involving two warming events
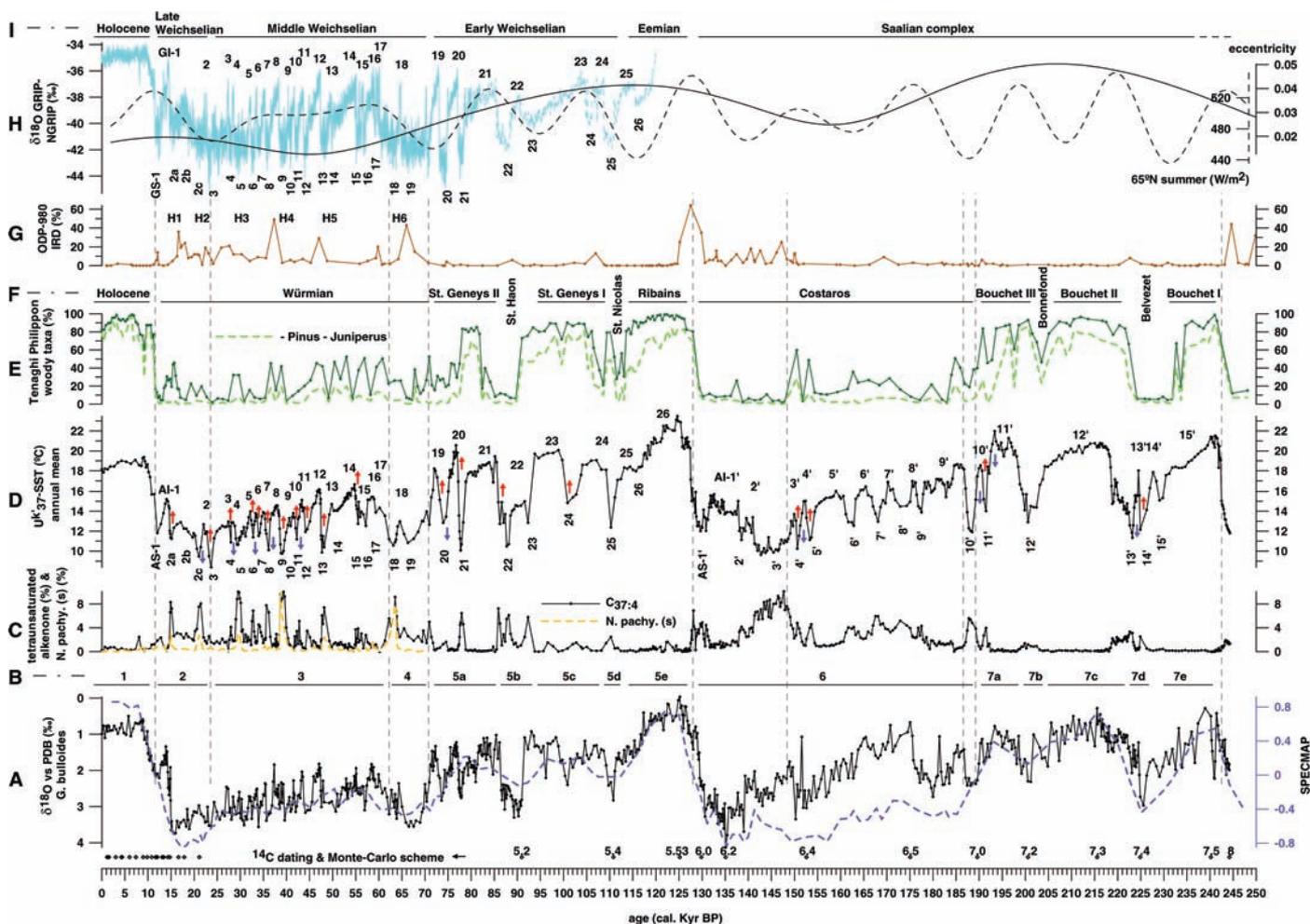


**Fig. 2.** Paleoenvironmental records of the last two interglacial-to-glacial cycles. (**A**) δ18O of *G. bulloides* in ODP-977A (*17*) compared with the SPECMAP standard isotope curve (*18*), which is shown by the dotted line. Diamonds show some of the control points used for the age model (*17*). (**B**) Glacial (2 to 4 and 6) and interglacial (1, 5, and 7) MISs. (**C**) Relative proportion of heptatriatetraenone to total alkenones. This biomarker may be used as a tracer of cold and/or low salinity waters at the Iberian margin (*29*). The percentage of *N. pachyderma* sinistral is also plotted for reference (*28*). (**D**) SST in ODP-977A (*17*). Twenty-six interstadials (AI-1 to 26) and stadials (AS-1 to 26) have been identified over the last climate cycle. The penultimate climate cycle exhibits 15 warm (AI-1′ to 15′) and 15 cold (AS-1′ to 15′) spells that are labeled following the scheme recommended by the INTIMATE group (*20*).

Abrupt changes are defined as warming (red arrows) or cooling (blue arrows) episodes that happen at a rate equal to or faster than the SST variation over the last deglaciation (2.6°C/ky) (table S1). (**E**) Tenaghi Philippon woody taxa, in addition to the temperate pollen curve shown by the dotted thick line, which excludes *Pinus* and *Juniperus* (*13*). (**F**) The Velay pollen sequence stratigraphy (*14*). (**G**) The relative proportion of detrital lithics (IRD) recorded at 55°N in the North Atlantic sediments (*6*). (**H**) The δ18O in GRIP and NGRIP with the isotopically defined Greenland interstadials (GI) on the top and the subsequent Greenland stadials (GS) on the bottom (*1*, *3*). The eccentricity of the Earth's orbit and the daily insolation at 65°N during the summer solstice are also shown (*36*). (**I**) The widely used northwest European terminology.

(AI-4′ and AI-3′) and one cooling event [AS-4′, 155 to 150 ka (Fig. 2D and table S1)]. These changes registered drops in SST as severe as those coinciding with HEs during MIS 3 and were concurrent with prominent increases of up to 60% in arboreal pollen documented in the Tenaghi Philippon profile (*13*) [mainly *Pinus* and *Juniperus* (Fig. 2E)]. This sequence of events was followed by a prolonged cold episode that went along with the dominance of low-salinity surface waters as displayed by increased percentages of $C_{37:4}$ [AS-3′, 149 to 141 ka (Fig. 2, C and D)]. Toward the end of MIS 6, IRD intervals were identified in the northeast Atlantic (*6, 30*) and the Labrador Sea (*31*). However, at the Iberian margin these events were less intense than those of the last glacial and uniquely European in origin (*11*). As discussed below, this result points to a spatial configuration in the frontal zones during the penultimate glacial that differs greatly from that of the last glacial (*32*).

One of the largest SST changes observed in the entire record occurred at the end of MIS 5 and involved an abrupt warming of 10.5°C in 1 ky and a subsequent cooling by −7.7°C in 2.8 ky [from AS-21 to AI-20 (table S1)]. This abrupt SST change was preceded by a prominent cooling (−9.4°C) after a long period of stability at warm SSTs (AI-21). Similar transitions are observed throughout MISs 5 and 7 (Fig. 2D). In four cases, these cooling transitions were abrupt (AI-20, 10′, 11′, and 13′; between −2.8 and −5.1°C/ky), whereas six abrupt warming transitions back to previous high SSTs were observed [AS-20, 21, 22, 24, 11′, and 14′; between 2.6 and 15.6°C/ky (table S1)]. The record from ODP-977A shows that major SST changes occurred within a few centuries and were often of larger magnitude than those in the glacial periods and comparable in amplitude to the glacial-to-interglacial warming. SST variability was associated with large shifts in mean annual air temperature and moisture as reflected in vegetational changes around the Mediterranean (*13, 14*), for example, St. Nicolas, Bonnefond, and Belvezet stadials (Fig. 2, E and F). One of the most extreme events, AS-22, is coincident with one of the longest cold phases in Southern European pollen sequences, St. Haon (*13, 14*), and in line with the maximum extension of the Barents-Kara and Scandinavian ice sheets at the Early Weichselian (*33*). This ice increase blocked the drainage of northeast European rivers owing to large proglacial lakes caused by strong regional summer cooling (*34*). During MISs 5 and 7, the iceberg discharges were drastically diminished (*6*) (Fig. 2G), which is most likely related to the scarcity of continental ice near the North Atlantic. Thus, even in the absence of large ice sheets (*6*) and major sea level fluctuations (*35*), dramatic

shifts in the climate occurred, indicating that episodic abrupt change is a fundamental aspect of Pleistocene climate (*6*). High amplitude SST variability during these relatively warm and largely ice-free periods disqualifies catastrophic meltwater discharge events as a driving force of these oscillations.

An abrupt change requires a trigger, an amplifier, a source of persistence, and a globalizer (*24*). In core ODP-977A, the higher number of abrupt events during MISs 2 to 4 compared with that in MIS 6 parallel the lower amplitude of the eccentricity of the Earth's orbit and the irradiance variations at high northern latitudes in summer (*36*) in the former but not in the latter period (Fig. 2, D and H). During MIS 2 to 4, a long-term lack of seasonal contrast enhanced the role of sea or land ice and the resulting southward displacement of frontal zones (*32*), bringing about more frequent arrivals of polar climate conditions at the latitude of study. The sensitivity of climate to change was less during MIS 6. It is highly probable that changes in thermohaline circulation were influential in causing persistent SST variability over these glacial stages. In the North Atlantic, differential solar heating between high and low latitudes tends to accelerate surface waters polewards, whereas freshwater input to high latitudes, together with low-latitude evaporation, tend to restrain this flow (*37*). Data and models both suggest that, in response to small changes in the hydrological cycle, the Atlantic meridional overturning circulation and the formation of North Atlantic Deep Water (NADW) contributed to sustaining rapid climate change during the last glaciation (*5, 37–39*). Ocean convection sites of NADW formation jumped between the Nordic seas and an area to the south of the Icelandic sill (*39*). Additionally, observational evidence and simulated climate conditions (*8, 16, 22, 23, 40, 41*) point to preponderant atmospheric mechanisms interacting with the oceanic mixed layer (e.g., strength of westerly, trade, or monsoon winds or southward migration of the Intertropical Convergence Zone) for the amplification and transmission of the D/O signal observed during the last glacial.

MISs 5 and 7 show continued stability in SST for long periods, for example, 10 ky, evolving rarely although dramatically to glacial conditions and, over a period of 1 to 2 ky, moving abruptly back to warm SST. During these periods, the eccentricity of the Earth's orbit and the seasonal contrast were more pronounced than in MISs 2 to 4 and MIS 6. These conditions and the strength of the NADW formation could have buffered development of the abrupt changes sustained by hydrological instability. Predictable orbital variations led to insolation changes, which triggered less frequent but very intense oscillations. Accord-

ingly, the last glacial inception (substage 5d) has been attributed to a connection between orbital forcing and thermohaline circulation beyond a freshwater threshold within the ocean-atmosphere-sea-ice system (*42, 43*).

If duration may be taken as a reference for stability, the ODP-977A record shows that the climate has been predominantly in interglacial-interstadial conditions over the past 250,000 years. The repeated saw-tooth morphology of recorded oscillations calls for strong positive feedback mechanisms to accelerate warming once the threshold is reached and the flip is triggered from one condition to another. Consequently, cold stadials were periods of only limited duration, immediately followed by well-defined returns to more warmth. In this respect, the Holocene shows a stable SST trend similar to those in previous interstadial stages, tending toward progressively cooler climate conditions in accordance with the slow decrease in summer insolation in the Northern Hemisphere and the minimal eccentricity of the Earth's orbit. Within the framework of ODP-977A data, this orbital configuration suggests that the present warm period could be more prone to abrupt oscillations than MISs 5 and 7. In turn, the next bifurcation of the climate system may appear as an extremely intense cooling if the future natural climate is going to develop as an analog of some of the preceding warm periods.

**References and Notes**

1. W. Dansgaard *et al.*, *Nature* **364**, 218 (1993).
2. P. M. Grootes, M. Stuiver, J. W. C. White, S. J. Johnsen, J. Jouzel, *Nature* **366**, 552 (1993).
3. North Greenland Ice Core Project members, *Nature* **431**, 147 (2004).
4. G. C. Bond *et al.*, *Nature* **365**, 143 (1993).
5. T. M. Dokken, E. Jansen, *Nature* **401**, 458 (1999).
6. J. F. McManus, D. W. Oppo, J. L. Cullen, *Science* **283**, 971 (1999).
7. J. F. McManus *et al.*, *Nature* **371**, 326 (1994).
8. I. Cacho *et al.*, *Paleoceanography* **14**, 698 (1999).
9. J. P. Sachs, S. J. Lehman, *Science* **286**, 756 (1999).
10. D. Pailler, E. Bard, *Palaeogeogr. Palaeoclimatol. Palaeoecol.* **181**, 431 (2002).
11. L. de Abreu, N. J. Shackleton, J. Schonfeld, M. A. Hall, M. Chapman, *Mar. Geol.* **196**, 1 (2003).
12. J. R. M. Allen *et al.*, *Nature* **400**, 740 (1999).
13. P. C. Tzedakis, J. F. McManus, H. Hooghiemstra, D. W. Oppo, T. A. Wijmstra, *Earth Planet. Sci. Lett.* **212**, 197 (2003).
14. M. Reille, J. L. de Beaulieu, H. Svobodova, V. Andrieu-Ponel, C. Goeury, *J. Quat. Sci.* **15**, 665 (2000).
15. D. Genty *et al.*, *Nature* **421**, 833 (2003).
16. M. Bar-Matthews, A. Ayalon, M. Gilmour, A. Matthews, C. J. Hawkesworth, *Geochim. Cosmochim. Acta* **67**, 3181 (2003).
17. Materials and methods are available as supporting material on *Science* Online.
18. D. G. Martinson *et al.*, *Quat. Res.* **27**, 1 (1987).
19. In continental studies, warming stages of limited duration are referred to as interstadials, whereas short-term cooling stages are known as stadials. The differentiation between interglacials and interstadials is only a matter of intensity and duration. Over the past 250,000 years, only the marine isotope substage 5e (Eemian) is clearly of an interglacial nature. To date, there is no general agreement in considering which of the marine isotope warm units (7a, 7c, and 7e) should be classed as interglacial and which as interstadial. In this study, all warm periods are referred to as interstadials.

20. M. J. C. Walker *et al.*, *Quat. Sci. Rev.* **18**, 1143 (1999).
21. N. Ohkouchi, T. I. Eglinton, L. D. Keigwin, J. M. Hayes, *Science* **298**, 1224 (2002); published online 10 October 2002 (10.1126/science.1075287).
22. L. C. Peterson, G. H. Haug, K. A. Hughen, U. Röhl, *Science* **290**, 1947 (2000).
23. D. W. Lea, D. K. Pak, L. C. Peterson, K. A. Hughen, *Science* **301**, 1361 (2003).
24. R. B. Alley *et al.*, *Science* **299**, 2005 (2003).
25. D. Rind, *Science* **296**, 673 (2002).
26. H. Heinrich, *Quat. Res.* **29**, 143 (1988).
27. O. Cayre, Y. Lancelot, E. Vicent, M. A. Hall, *Paleoceanography* **14**, 384 (1999).
28. M. Perez-Folgado *et al.*, *Mar. Micropaleontol.* **48**, 49 (2003).
29. E. Bard, F. Rostek, J. L. Turon, S. Gendreau, *Science* **289**, 1321 (2000).
30. S. A. van Kreveld, M. Knappertsbusch, J. Ottens, G. M. Ganssen, J. E. van Hinte, *Mar. Geol.* **131**, 21 (1996).
31. R. N. Hiscott, A. E. Aksu, P. J. Mudie, D. F. Parsons, *Global Planet. Change* **28**, 227 (2001).
32. E. Calvo, J. Villanueva, J. O. Grimalt, A. Boelaert, L. D. Labeyrie, *Earth Planet. Sci. Lett.* **188**, 509 (2001).
33. J. I. Svendsen *et al.*, *Boreas* **28**, 234 (1999).
34. G. Krinner *et al.*, *Nature* **427**, 429 (2004).
35. M. Siddall *et al.*, *Nature* **423**, 853 (2003).
36. A. L. Berger, *J. Atmos. Sci.* **35**, 2362 (1978).
37. P. U. Clark, N. G. Pisias, T. F. Stocker, A. J. Weaver, *Nature* **415**, 863 (2002).
38. P. U. Clark *et al.*, *Science* **293**, 283 (2001).
39. A. Ganopolsky, S. Rahmstorf, *Nature* **409**, 153 (2001).
40. M. F. Sánchez-Goñi *et al.*, *Clim. Dyn.* **19**, 95 (2002).
41. J. C. H. Chiang, M. Biasutti, D. S. Battisti, *Paleoceanography* **18**, 41094 (2003).
42. M. Khodri *et al.*, *Nature* **410**, 570 (2001).
43. J. F. McManus, D. W. Oppo, L. D. Keigwin, J. L. Cullen, G. C. Bond, *Quat. Res.* **58**, 17 (2002).
44. We thank M. Hutterli and J. Schwander for providing the Monte Carlo wiggle-matched age scale, P. C. Tzedakis

# Efficient Deactivation of a Model Base Pair via Excited-State Hydrogen Transfer

**Thomas Schultz,[1]\* Elena Samoylova,[1] Wolfgang Radloff,[1] Ingolf V. Hertel,[1] Andrzej L. Sobolewski,[2] Wolfgang Domcke[3]**

We present experimental and theoretical evidence for an excited-state deactivation mechanism specific to hydrogen-bonded aromatic dimers, which may account, in part, for the photostability of the Watson-Crick base pairs in DNA. Femtosecond time-resolved mass spectroscopy of 2-aminopyridine clusters reveals an excited-state lifetime of $65 \pm 10$ picoseconds for the near-planar hydrogen-bonded dimer, which is significantly shorter than the lifetime of either the monomer or the 3- and 4-membered nonplanar clusters. Ab initio calculations of reaction pathways and potential-energy profiles identify the mechanism of the enhanced excited-state decay of the dimer: Conical intersections connect the locally excited $^1\pi\pi^*$ state and the electronic ground state with a $^1\pi\pi^*$ charge-transfer state that is strongly stabilized by the transfer of a proton.

An important property of DNA is its robustness with respect to damage by the harmful ultraviolet (UV) components [wavelength ($\lambda$) $< 400$ nm] of sunlight. The solar UV photons are ubiquitous and potent mutagens, which have accompanied the development of life for billions of years.

The $^1\pi\pi^*$ excited states of the DNA bases that are accessed by UV absorption lie approximately 5 eV above the ground state. The significant energy deposited in the molecule by UV radiation could initiate a variety of photochemical reactions. The available data (*1*) indicate that these reactive decay channels are efficiently quenched by fast radiationless decay back to the electronic ground state (termed internal conversion). These mechanisms provide DNA with a high degree of intrinsic photostability. The origin of rapid internal conversion within DNA could involve the interplay of the sugar-phosphate backbone, the hydrogen bonding of the Watson-Crick (WC) base pairs, stacking interactions, and solvation. Following a reductionistic approach, we focus here on whether isolated WC base pairs show greater photostability than do individual bases.

Several groups recently used ab initio calculations (*2–4*) and time-resolved spectroscopy (*1*) to identify specific radiationless-decay mechanisms in isolated DNA bases. However, experimental investigation of the excited-state lifetime of WC base pairs is complicated by several factors. Most importantly, the excited-state lifetimes of the monomers are already very short (*1*), and there exist several tautomeric forms of the isolated WC base pairs (*5*). Simplified mimetic

models of WC base pairs allow the investigation of some of the basic photochemical reaction mechanisms without these complexities. An extensively studied reaction is double proton transfer in the mimetic model 7-azaindole dimer (*6*). Recent ab initio calculations for the guanine-cytosine (GC) base pair, however, suggest a hydrogen-atom transfer reaction involving amino groups as proton donors and ring nitrogens as proton acceptors (*7*). Near the hydrogen-transfer minimum, a conical intersection with the electronic ground state leads to rapid internal conversion. This reaction can be studied in the model compound 2-aminopyridine (2AP) dimer, which offers the relevant hydrogen bonds and reaction pathways (*8*) but otherwise lacks the complexity of the pyrimidine and purine bases. Theory predicts near-planar hydrogen-bonded structures for DNA base pairs (*7, 9*) as well as for the 2AP dimer (*8*).

We employed pump-probe ionization spectroscopy to characterize the excited-state properties of 2AP clusters (Fig. 1A). The clusters were formed in a pulsed supersonic jet expansion of 2AP, seeded in 1 bar of helium. The size distribution $[(2AP)_n]$ of the clusters was controlled by heating the 2AP sample to the 30° to 80°C range. Molecules and clusters were photoexcited by a femtosecond laser pump pulse at 293, 274, or 250 nm, then ionized by a delayed probe pulse at 200 or 800 nm, and finally mass-analyzed in a time-of-flight mass spectrometer. Clustering conditions were varied to obtain very narrow cluster size $n$ ($n \le 2$ molecules) or broad ($n = 1$ to 8) cluster distributions to diagnose cluster fragmentation effects.

In the mass spectrum with broad cluster distribution (Fig. 1B) obtained by excitation with a 274-nm pulse and three-photon ionization with an 800-nm pulse, the magnitude of the ion signal was directly proportional to the number of molecules in the excited state. Measurement of a chosen ion signal as a function of the pump-probe delay thus allowed for the characterization of the

[1]Max Born Institute Berlin, Max-Born-Straße 2a, D-10247 Berlin, Germany. [2]Institute of Physics, Polish Academy of Sciences, Aleja Lotnikow 32/46, PL-02668 Warsaw, Poland. [3]Department of Chemistry, Technical University of Munich, Lichtenbergstraße 4, D-85747 Garching, Germany.

\*To whom correspondence should be addressed. E-mail: schultz@mbi-berlin.de